DOI: 10.1002/ejic.200500667

Peculiarities of the Synthesis of Lithium Ion Conducting Lanthanum Tantalate by Solid-State Reaction and Precipitation from Solutions

Anatolii Belous,*[a] Oksana Gavrilenko,[a] Olena Pashkova,[a] Cyrille Galven,[b] and Odile Bohnké[b]

Keywords: Tantalates / Solid-state reactions / Precipitation from solution / Microstructure / Ionic conductivity

Synthesis of lithium ion conducting tantalates has been carried out by conventional solid-state reaction (SSR) techniques and by precipitation from solutions (PS). It is shown that the latter chemical route leads to the formation of a pure perovskite phase, made up of nanosized particles, and uses milder conditions when compared with the solid-state reaction technique. Thermal analyses, X-ray powder diffraction (XRD) and infrared (IR) spectroscopy are used to investigate the phase transformations that occur during the preparation of these tantalates from powder precursors. After sintering, the nanosized particles of the powder obtained by the (PS) route are preserved and pellets with good compactness (89 %) are obtained. The electrical properties of the sintered ceramics have been investigated by ac impedance spectroscopy. These experiments showed that the total ionic conductivity (bulk and grain boundaries) of the (PS) pellet is slightly lower than that of the (SSR) pellet. This decrease of conductivity is attributed to an enhancement of the blocking effect of the grain boundaries resulting from the microstructure of the fine-grain ceramics. The bulk conductivity is not affected by the synthetic route.

Introduction

Much attention is given to the investigation of solid-state lithium ion conductors because of their potential use in electrochemical devices as solid electrolytes, electrodes or ion-selective membranes. The lithium containing lanthanum titanates, which have a defect perovskite structure $(Li_{3x}La_{4/3-x}v_{2/3-2x})Ti_2O_6$ (v = vacancy), have deserved much attention these last years because of their high ionic conductivity of 10^{-3} S·cm^{-1} at 300 K.[1–3] Apart from the titanate perovskites, the lithium-containing lanthanum tantalates, which also display a defect perovskite structure $(Li_{3x}La_{2/3-x}v_{4/3-2x})Ta_2O_6$ with a large number of vacancies, show an ionic conductivity of 10^{-4} S·cm^{-1} at 300 K, only one order of magnitude smaller than the ionic conductivity of the titanates. The crystallographic structure and transport properties of these tantalates prepared by solid-state reactions have already been studied.[4–8] However, the details and peculiarities of the different chemical reactions and phase transformation occurring during the synthesis of the lanthanum tantalate $(La_{2/3}v_{4/3})Ta_2O_6$ and the lithium-containing lanthanum tantalates $(Li_{3x}La_{2/3-x}v_{4/3-2x})Ta_2O_6$ have never been considered. This is the main purpose of this work. Furthermore, since it is clearly established that the method of synthesis affects the microstructure and consequently the properties of the oxides, we investigated two different methods of synthesis: the precipitation from solution (PS) and the more conventional solid-state reaction (SSR) methods. An advantage of the (PS) method is the possibility to greatly reduce the synthesis temperature and also to produce nanosized particles.[9]

The aim of the present work is then to investigate the phase transformations occurring during the synthesis of lithium-containing lanthanum tantalate $(Li_{3x}La_{2/3-x}v_{4/3-2x})Ta_2O_6$ either by the solid-state reaction (SSR) technique or by precipitation from solution (PS), and to study the effect of the synthetic method on the microstructure and the electrophysical properties of these tantalates.

Results And Discussion

Synthesis

Solid-State Reaction (SSR) Method

According to the results of the XRD analysis, the mixture of the original reagents after a mild homogenisation consists of monoclinic Li_2CO_3 (for lithium-containing samples), hexagonal $La(OH)_3$ and orthorhombic Ta_2O_5. Figure 1 (a) shows DTA, DTG and TG curves for four mixtures of the original reagents with different lithium contents: $3x = 0$ (curve 1), 0.50 (curve 2), 1.10 (curve 3) and

[a] V.I.Vernadskii Institute of General and Inorganic Chemistry, 32/34 Palladina Avenue, 03680 Kyiv, 142 Ukraine
Fax: +380-42-42-211
E-mail: a.belous@list.ru
[b] Institut de Recherche en Ingénierie Moléculaire et Matériaux Fonctionnels FR CNRS 2575, Laboratoire des Oxydes et Fluorures (UMR, 6010 CNRS), Université du Maine, Avenue O. Messiaen, 72085 Le Mans Cedex 9, France

1.85 (curve 4). The DTG curves display four loss peaks, which are accompanied by endothermic reactions, as shown in the DTA. The first peak at 620–650 K (A), which decreases with x content and disappears in curve 4 when La is almost absent, can be attributed to $La(OH)_3$ dehydration. The second one at 910–990 K (B), which does not appear in curve 1 when Li is absent and that increases with x content, is attributed to Li_2CO_3 thermolysis. As the Li_2CO_3 content increases (curves 2 to 4), the initial Li_2CO_3 decomposition temperature range increases and the decomposition rate increases. For instance, for $(Li_{3x}La_{2/3-x}v_{4/3-2x})Ta_2O_6$ samples at $3x = 0.50$, 1.10 and 1.85, the Li_2CO_3 decomposition temperature range becomes wider: from 820–990 K to 770–990 K and finally to 720–990 K, respectively. Finally, the two other peaks, marked as (∗) and (o) on the curves, can be attributed to the partial (700–800 K) and complete (1050–1075 K) $La_2O_2CO_3$ decarbonation. The appearance of lanthanum dioxomonocarbonate has been proved by XRD analysis on samples calcined at 770 K. The complete decomposition temperature of lanthanum dioxomonocarbonate decarbonation in lithium-containing samples shifts towards higher temperatures as compared with the basic $La_{2/3}Ta_2O_6$ sample. This is accounted for by the fact that the thermal decomposition of dioxomonocarbonate slows down in an atmosphere rich in CO_2.[10]

Figure 1 (b) shows IR spectra, recorded at room temperature, of raw materials Ta_2O_5 (curve 1), La_2O_3 (curve 2), Li_2CO_3 (curve 3) and of their homogenised mixtures (curves 4–7). The IR spectra of the mixtures (curves 4–7) are characterised by a superposition of absorption bands, which are typical of the spectra of original reagents. However, small shifts can be observed. The stretching vibration band of the CO groups, observed at 1480 cm^{-1} in pure Li_2CO_3, shifts slightly towards higher frequencies.[11] Furthermore, the deformation vibration δ band and stretching vibration v band of Ta–O observed at 355 cm^{-1} and 555 cm^{-1}, respectively, in pure Ta_2O_5, shift to higher and lower frequencies, respectively. The shifts depend on the Li content ($3x$). For instance, the Ta–O vibration frequencies of samples at $3x = 0$, 0.50, 1.10, 1.85 are observed at 355 and 555 cm^{-1}, 368 and 545 cm^{-1}, 375 and 525 cm^{-1}, 380 and 510 cm^{-1}, respectively. From these results, it can be inferred that the system obtained after homogenising milling differs from a simple mixing of the original reagents.

Powder XRD spectra have been recorded at room temperature on powders as a function of composition and firing temperature, in the temperature range from 370 K to 1770 K. The results are summarised in Table 1. From these results, it is evident that during the formation of the lanthanum metatantalate with a defect perovskite structure of the composition $La_{2/3}Ta_2O_6$ ($3x = 0$) the reaction between lanthanum oxide and tantalum oxide begins at 1320 K, and carries on actively at temperatures above 1470 K. According to the XRD spectra analysis, the synthesis proceeds via the formation of intermediate phases: monoclinic lanthanum orthotantalate ($LaTaO_4$), orthorhombic lanthanum heptatantalate ($LaTa_7O_{19}$) and pentatantalate ($LaTa_5O_{14}$).[12] Lanthanum metatantalate as the main phase

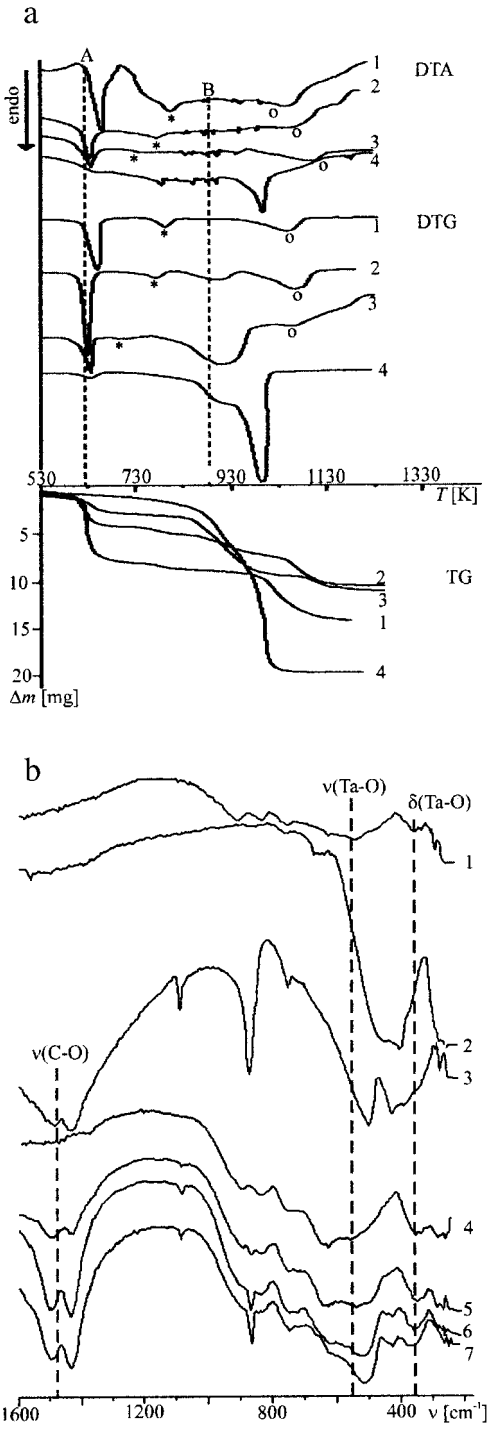

Figure 1. (a) Thermal analyses of the mixture of original reagents, with different lithium contents, for the synthesis by the (SSR) route of $(Li_{3x}La_{2/3-x}v_{4/3-2x})Ta_2O_6$: (1) $3x = 0$, (2) $3x = 0.50$, (3) $3x = 1.10$, (4) $3x = 1.85$. (b) IR spectra, recorded at room temperature, of the original reagents (1) Ta_2O_5, (2) La_2O_3, (3) Li_2CO_3 and of their homogenised mixtures, with different lithium contents, for the synthesis by the (SSR) route of $(Li_{3x}La_{2/3-x}v_{4/3-2x})Ta_2O_6$: (4) $3x = 0$, (5) $3x = 0.50$, (6) $3x = 1.10$, (7) $3x = 1.85$.

was found in the samples calcined at 1570 K. At 1770 K, the yield of the phase with the perovskite structure is 95% (Table 1). It is obvious that a higher temperature is required for the complete reaction of formation of $La_{2/3}Ta_2O_6$ by the

Table 1. Phase composition of the $(Li_{3x}La_{2/3-x}v_{4/3-2x})Ta_2O_6$ powder prepared by the (SSR) route as a function of lithium content, $3x$, and firing temperature, T (the firing time is 1 h). The different phases are given in the order of their decreasing amount.

T [K]	$3x = 0$	$3x = 0.50$	$3x = 0.62$	$3x = 0.74$	$3x = 1.10$
370	Ta_2O_5 $La(OH)_3$	Ta_2O_5 $La(OH)_3$ Li_2CO_3	Ta_2O_5 $La(OH)_3$ Li_2CO_3	Ta_2O_5 $La(OH)_3$ Li_2CO_3	Ta_2O_5 $La(OH)_3$ Li_2CO_3
770	Ta_2O_5 $La(OH)_3$ $La_2O_2CO_3$	Ta_2O_5 $La_2O_2CO_3$ $LiTaO_3$	Ta_2O_5 $La_2O_2CO_3$ $LiTaO_3$	Ta_2O_5 $La_2O_2CO_3$ $LiTaO_3$	Ta_2O_5 $LiTaO_3$ Li_2CO_3 $La_2O_2CO_3$
970	Ta_2O_5 La_2O_3	Ta_2O_5 $LiTaO_3$ La_2O_3 La_3TaO_7	Ta_2O_5 $LiTaO_3$ La_2O_3 La_3TaO_7	$LiTaO_3$ Ta_2O_5 La_2O_3 La_3TaO_7	$LiTaO_3$ Ta_2O_5 La_2O_3 La_3TaO_7
1220	Ta_2O_5 La_2O_3	Ta_2O_5 $LiTaO_3$ La_2O_3 $LiTa_3O_8$ perovskite $LaTaO_4$	$LiTaO_3$ Ta_2O_5 $LiTa_3O_8$ La_2O_3 perovskite $LaTaO_4$	$LiTaO_3$ Ta_2O_5 $LiTa_3O_8$ La_2O_3 perovskite $LaTaO_4$	–
1320	Ta_2O_5 $LaTa_7O_{19}$ perovskite $LaTa_5O_{14}$ $LaTaO_4$	Ta_2O_5 $LiTaO_3$ perovskite $LiTa_3O_8$ $LaTaO_4$ $LaTa_5O_{14}$	$LiTaO_3$ Ta_2O_5 perovskite $LiTa_3O_8$ $LaTa_5O_{14}$ $LaTaO_4$	$LiTaO_3$ Ta_2O_5 $LiTa_3O_8$ perovskite $LaTa_5O_{14}$ $LaTaO_4$	$LiTaO_3$ Ta_2O_5 $LiTa_3O_8$ perovskite $LaTa_5O_{14}$ $LaTaO_4$
1420	Ta_2O_5 perovskite $LaTa_7O_{19}$ $LaTa_5O_{14}$ $LaTaO_4$	$LiTa_3O_8$ Ta_2O_5 perovskite $LiTaO_3$ $LaTaO_4$ $LaTa_5O_{14}$	$LiTaO_3$ $LiTa_3O_8$ Ta_2O_5 perovskite $LaTa_5O_{14}$ $LaTaO_4$		
1570	perovskite Ta_2O_5 $LaTa_5O_{14}$ $LaTaO_4$	perovskite $LiTa_3O_8$ $LiTaO_3$ $LaTaO_4$ Ta_2O_5	$LiTaO_3$ $LiTa_3O_8$ Ta_2O_5 perovskite $LaTa_5O_{14}$ $LaTaO_4$	$LiTaO_3$ Ta_2O_5 $LiTa_3O_8$ perovskite $LaTaO_4$ $LaTa_5O_{14}$	$LiTaO_3$ perovskite
1770	perovskite $LaTa_5O_{14}$ (4.8%)	perovskite $LaTa_5O_{14}$ (7.7%)	perovskite $LaTa_5O_{14}$ (3.3%)	perovskite $LiTaO_3$ (4%)	perovskite $LiTaO_3$ (37%)

SSR method. According to Portnoi et al. this temperature is 1870 K.[13] On the basis of the analysis of the phase composition and phase ratio as a function of firing temperature (Table 1) and taking into account the literature data,[14,15] the process of formation of lanthanum metatantalate, $La_{2/3}Ta_2O_6$ ($LaTa_3O_9$), with a defect perovskite structure of the tetragonal system, may be represented by Equations (1), (2), (3), (4) and (5).

$$La_2O_3 + Ta_2O_5 \xrightarrow{1320-1570\ K} 2\ LaTaO_4 \quad (1)$$

$$LaTaO_4 + Ta_2O_5 \xrightarrow{1320-1570\ K} LaTa_3O_9 \quad (2)$$

$$LaTa_3O_9 + Ta_2O_5 \xrightarrow{1320-1420\ K} LaTa_5O_{14} \quad (3)$$

For lithium-containing samples $(Li_{3x}La_{2/3-x}v_{4/3-2x})Ta_2O_6$, the primary phase that appears in the process of

$$LaTa_5O_{14} + Ta_2O_5 \underset{1470-1570\ K}{\overset{1320-1420\ K}{\rightleftharpoons}} LaTa_7O_{19} \quad (4)$$

$$LaTa_5O_{14} + LaTaO_4 \xrightarrow{1320-1770\ K} 2\ LaTa_3O_9 \quad (5)$$

heat treatment of a homogenised mixture of original reagents is lithium metatantalate ($LiTaO_3$) of the rhombohedral system, which appears in diffractograms of samples fired at 770 K [Equation (6)].

$$Li_2O + Ta_2O_5 \xrightarrow{770-1320\ K} 2\ LiTaO_3 \quad (6)$$

When the temperature is raised to 1170 K, the amount of $LiTaO_3$ increases and an orthorhombic lanthanum paratantalate (La_3TaO_7) phase appears [Equation (7)].

$$3\ La_2O_3 + Ta_2O_5 \xrightarrow{770-1170\ K} 2\ La_3TaO_7 \quad (7)$$

The La_3TaO_7 phase transforms into the lanthanum orthotantalate ($LaTaO_4$) for the temperature range 1170–1220 K. During the synthesis of $La_{2/3}Ta_2O_6$ ($3x = 0$), $LaTaO_4$ is formed at 1320 K (Table 1). Therefore, its appearance at a lower temperature (1220 K) in lithium-containing samples is probably due to the decomposition of La_3TaO_7 as expressed by Equation (8).[14]

$$La_3TaO_7 \xrightarrow{1170-1220\ K} La_2O_3 + LaTaO_4 \quad (8)$$

At 1220 K, $LiTaO_3$ from Equation (6) as well as La_2O_3 and $LaTaO_4$ from Equation (8) can react partially with the remaining Ta_2O_5 to form the monoclinic phase of lithium polytantalate $LiTa_3O_8$, $LaTaO_4$ and $LaTa_3O_9$, respectively, according to the following reactions, Equations (9), (10) and (11).

$$LiTaO_3 + Ta_2O_5 \underset{1450-1600\ K}{\overset{1220-1420\ K}{\rightleftharpoons}} LiTa_3O_8 \quad (9)$$

$$La_2O_3 + Ta_2O_5 \xrightarrow{1220-1320\ K} 2\ LaTaO_4 \quad (10)$$

$$LaTaO_4 + Ta_2O_5 \xrightarrow{1220-1570\ K} LaTa_3O_9 \quad (11)$$

At the same time, $LiTaO_3$ and $LaTa_3O_9$ react to form the lithium-containing metatantalates (P) with the perovskite structure.

When the temperature is raised to 1320 K, the $LaTa_5O_{14}$ phase begins to form in addition to the above-mentioned phases [Equation (12)].

$$LaTa_3O_9 + Ta_2O_5 \xrightarrow{1320-1770\ K} LaTa_5O_{14} \quad (12)$$

This phase can react with $LaTaO_4$ to form $LaTa_3O_9$ [Equation (13)].

$$LaTa_5O_{14} + LaTaO_4 \xrightarrow{1320–1770\ K} 2\ LaTa_3O_9 \quad (13)$$

It should be noted that in the diffractograms of all the samples fired at 1320 K and higher, the diffraction lines typical of the high-temperature modification (F1) of tantalum(v) oxide appear in addition to the lines resulting from the low-temperature modification (F) of Ta_2O_5[12] (Figure 2, a). The appearance of a defect-perovskite structure in lithium-containing samples is observed at 1220 K, which is 100 K lower than the initial formation temperature in the synthesis of $La_{2/3}Ta_2O_6$ ($3x = 0$). As generally observed in Ca tantalates[16] or La titanates,[17] the addition of lithium greatly decreases the required synthesis temperature of the perovskite compounds.

Figure 2 (a) shows diffractograms recorded at room temperature in the 2θ range from 20° to 40° of $Li_{0.5}La_{0.5}Ta_2O_6$ ($3x = 0.5$) samples fired at and above 1320 K. As discussed previously, at 1320 K the formation of the perovskite phase (P) can be observed by the appearance of the diffraction line at $2\theta = 32.5°$. All the other phases are present: Ta_2O_5 (F and F1), $LiTaO_3$ (B), $LaTaO_4$ (C), the monoclinic form of $LiTa_3O_8$ (G1) and $LaTa_5O_{14}$ (D) in a small amount. As temperature increases, the amount of perovskite (P) increases. The formation of lithium-containing metatantalates (P) is accompanied by a consumption of the phases Ta_2O_5 (F1), $LiTaO_3$ (B), $LaTaO_4$ (C) and $LiTa_3O_8$ (G1 and G2). At 1770 K, a $Li_{0.5}La_{0.5}Ta_2O_6$ sample containing 92.3% of the perovskite phase is obtained with 7.7% of the $LaTa_5O_{14}$ phase. It is obvious that the temperature of 1770 K is not sufficient for the completion of the reaction, as in the case of the synthesis of lithium-free lanthanum metatantalate. A higher yield of 96–97% of the perovskite phase (P) can be achieved for higher lithium content ($0.5 < 3x < 1$). As $3x$ increases, the impurity phase observed at 1770 K changes from $LaTa_5O_{14}$ to $LiTaO_3$. This is clearly shown in Figure 2 (b), which shows fragments of diffractograms of $La_{0.3}Li_{1.1}Ta_2O_6$ ($3x = 1.1$) samples fired at 1320, 1570 and 1770 K. The presence of $LaTa_5O_{14}$ as the impurity can be explained by the existence of a partial reaction [Equation (13)] when $3x$ is small. At 1320 K, the formation of the perovskite phase (P) is observed with the presence of all the above-mentioned phases (F), (B) in a greater amount, (C), (G1) and (D). A two-phase sample (perovskite and $LiTaO_3$) is obtained at 1570 K. An increase in the amount of the perovskite phase (P) accompanied by a decrease in the amount of $LiTaO_3$ (B) in the two-phase sample, over the temperature range 1570–1770 K, demonstrates unambiguously that lithium metatantalate ($LiTaO_3$) is involved in the reaction.

The end reaction of lanthanum-lithium metatantalate formation may proceed according to Equation (14).

$$(2/3\text{-}x)\ LaTa_3O_9 + 3x\ LiTaO_3 \xrightarrow{1220–1770\ K} Li_{3x}La_{2/3\text{-}x}Ta_2O_6 \quad (14)$$

Thus, it has been found that the processes of formation of lanthanum metatantalate and lithium-containing lanthanum metatantalate proceed via the formation of the intermediate phases $LaTaO_4$, $LaTa_5O_{14}$, $LaTa_7O_{19}$ and $LiTaO_3$, $LiTa_3O_8$, $LaTaO_4$, $LaTa_3O_9$, $LaTa_5O_{14}$, respectively. This complex multistep mechanism of the formation of $(Li_{3x}La_{2/3-x}v_{4/3-2x})Ta_2O_6$ by the SSR method predetermines the micro heterogeneity of the obtained materials and calls for prolonged soaking at high temperature.

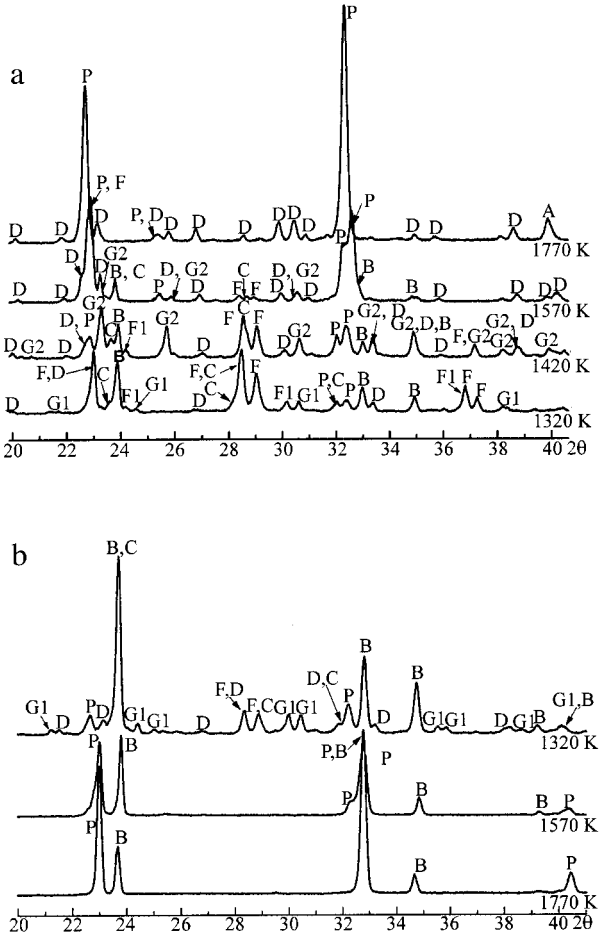

Figure 2. (a) Powder XRD spectra, recorded at room temperature, of $Li_{0.5}La_{0.5}Ta_2O_6$ prepared by the (SSR) technique and fired at different temperatures. P = perovskite, B = $LiTaO_3$, C = $LaTaO_4$, D = $LaTa_5O_{14}$, F = Ta_2O_5 (low temperature form), F1 = Ta_2O_5 (high temperature form), G1 = $LiTa_3O_8$ (monoclinic), G2 = $LiTa_3O_8$ (orthorhombic). (b) Powder XRD spectra, recorded at room temperature, of $Li_{0.3}La_{1.1}Ta_2O_6$ prepared by the (SSR) technique and fired at different temperatures. P = perovskite, B = $LiTaO_3$, C = $LaTaO_4$, D = $LaTa_5O_{14}$, F = Ta_2O_5 (low temperature form), G1 = $LiTa_3O_8$ (monoclinic).

Precipitation from Solution (PS) Method

The results of the thermal investigation (DTA) of lanthanum and tantalum hydroxides and the product of their co-precipitation after addition of a stoichiometric amount of lithium hydroxide $(LLTaO)_{PS}$ are presented in Figure 3 (a). An examination of the heating curves for $(LLTaO)_{PS}$ (curve 3) showed the absence of thermoeffects inherent for individual hydroxides. Therefore it was suggested from thermal analysis that when the (PS) method is used the starting

powder of precursors $(LLTaO)_{PS}$ is not a mechanical mixture of hydroxides. The dehydration and decarbonation processes, which are accompanied by endothermic peaks observed in the thermogram of $(LLTaO)_{PS}$, occur until the crystallisation of the mixture and separation of a lithium metatantalate phase takes place (exothermic peak at 920 K) (see part a in Figure 3 and Table 2). In this case, the most intensive decrease in weight, resulting from the loss of CO_2 and H_2O, is accompanied by a broad endothermic peak with a maximum at 390 K. It should be noted that the $(LLTaO)_{PS}$ dehydration and decarbonation temperatures are lower than those for hydroxides [410 K and 450 K for $La(OH)_3{\cdot}nH_2O$ and $Ta_2O_5{\cdot}nH_2O$, respectively, Figure 3 (a)], which is apparently accounted for by the peculiar nature of the product obtained.

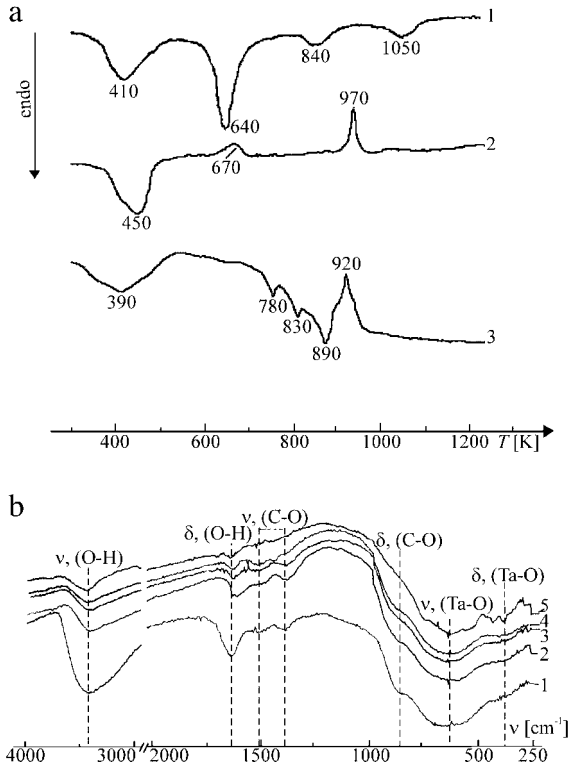

Figure 3. (a) Thermal analyses (DTA) of samples of (1) $La(OH)_3{\cdot}nH_2O$, (2) $Ta_2O_5{\cdot}nH_2O$ and (3) $Li_{0.5}La_{0.5}Ta_2O_6$, prepared by the (PS) route [$(LLTaO)_{PS}$]. (b) IR spectra, recorded at room temperature, of $Li_{0.5}La_{0.5}Ta_2O_6$ prepared by the (PS) route [$(LLTaO)_{PS}$] and fired at different temperatures: (1) 370 K, (2) 470 K, (3) 570 K, (4) 670 K and (5) 1020 K for 1 h.

The results of the IR spectroscopy of $(LLTaO)_{PS}$ over a wide-temperature range indicate the absence of the absorption bands that are characteristic of lanthanum and tantalum hydroxides,[18,19] which confirms the formation of new compounds during precipitation (Figure 3, b). The presence of a broad and intense absorption band with a maximum at 630 cm^{-1}, which corresponds to the Ta–O stretching vibration ν and shifts to 660 cm^{-1} with increasing firing temperature, is typical of the octahedral coordination of Ta atoms and indicates the presence of O–Ta–O bridge bonds of the polymeric type.[20] The band of the Ta–O deformation vibration δ at 350–380 cm^{-1} is poorly defined at low temperatures (part b of Figure 3, curves 1–4) but is well defined at 1020 K (part b of Figure 3, curve 5), which is the onset temperature for the formation of the defect perovskite structure (Table 2). The IR spectra of $(LLTaO)_{PS}$ are characterised by the presence of intense absorption bands at 3400–3440 cm^{-1} and 1600–1640 cm^{-1}, which correspond to stretching and deformation vibrations of H_2O molecules, respectively. Their frequencies depend weakly on the degree of hydration of samples, indicating that the bond energy of H_2O molecules in $(LLTaO)_{PS}$ does not vary (Figure 3, b). The high adsorption power of this system with respect to CO_2 is corroborated by the existence of stretching vibrations (ν) of the CO bond, at 1380–1520 cm^{-1}, and a shoulder at 850 cm^{-1}, which relates to deformation vibrations (δ) of CO groups and undergoes a considerable high-frequency shift (to 930 cm^{-1}) in the crystalline sample containing the perovskite phase (part b of Figure 3, curve 5).

Table 2. Phase composition of the $Li_{0.5}La_{0.5}Ta_2O_6$ powder prepared by the (PS) route $(LLTaO)_{PS}$ as a function of firing temperature, T (the firing time is 1 h). The different phases are given in the order of their decreasing amount.

T [K]	Phase composition
770	X-ray amorphous state
920	$LiTaO_3$
	X-ray amorphous phase
1020	$LiTaO_3$
	perovskite
	$LiTa_3O_8$
	X-ray amorphous phase
1070	$LiTaO_3$
	perovskite
	$LiTa_3O_8$
1120	perovskite
	$LiTaO_3$
	$LiTa_3O_8$
1170	perovskite
	$LiTaO_3$
	$LiTa_3O_8$
1270	perovskite
	$LiTaO_3$
1320	perovskite
	$LiTaO_3$
1370	perovskite
	$LiTaO_3$
1570	perovskite
	$LiTaO_3$
1670	perovskite

Thus on the basis of the results of the thermal analysis and IR spectroscopy it was concluded that when the PS method is used, the starting powder of precursors $(LLTaO)_{PS}$ obtained for the synthesis of lithium-containing lanthanum tantalate differs from the mechanical mixture of individual hydroxides and is an aquacomplex-type "inorganic polymer".[18]

The analysis of the XRD patterns of the $(LLTaO)_{PS}$ powders, fired at different temperatures (Figure 4 and Table 2), showed that the crystallization of the mixture, involving the formation of a lithium metatantalate phase, takes place at

920 K (Table 2). Several differences can be noted between the two synthetic methods. When the (PS) method is used, (i) the onset temperature of the defect-perovskite phase formation, from $(LLTaO)_{PS}$ powder, is 1020 K, which is 200 K lower than in the case for the synthesis by the SSR method (Table 1), (ii) the perovskite phase becomes predominant at 1120 K, instead of 1570 K for the (SSR) synthesis, (iii) the final firing temperature of the $Li_{0.5}La_{0.5}Ta_2O_6$ powder (1670 K) is decreased by 100 K (Table 1 and Table 2), (iv) the product obtained has a single phase, whereas the sample obtained by the SSR method contains a $LaTa_5O_{14}$ phase in addition to the perovskite (Table 1, Table 2; part a of Figure 2 and Figure 4). The observed considerable increase in the rate of chemical processes, when using the (PS) synthesis method, is because of the larger surface energy of the $(LLTaO)_{PS}$ powder and hence to a greater reactivity of the precursors.

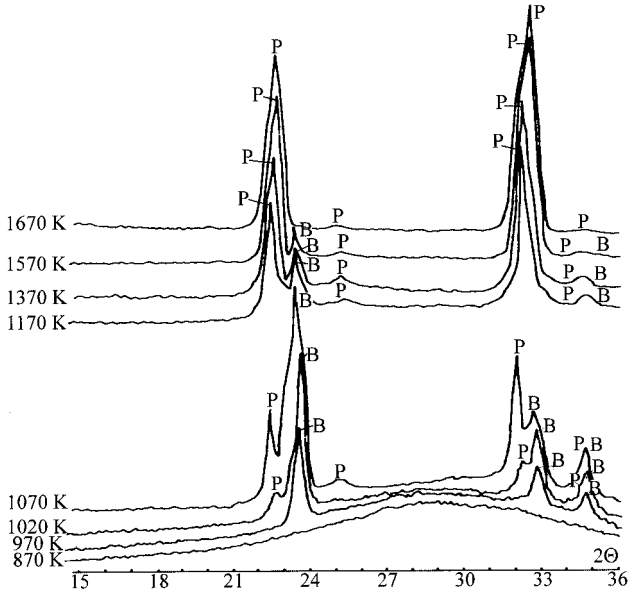

Figure 4. Powder XRD spectra, recorded at room temperature, of $Li_{0.5}La_{0.5}Ta_2O_6$ prepared by the (PS) route ($(LLTaO)_{PS}$) and fired at different temperatures. P = perovskite, B = $LiTaO_3$.

The Fullprof Rietveld analysis of the patterns collected from (SSR)[21] as well as from (PS) sintering samples indicated the formation of the defect-perovskite structure with tetragonal symmetry and the lattice parameters: $a = b = 3.903$ Å, $c = 7.831$ Å, $V = 119.29$ Å^3 and $a = b = 3.896$ Å, $c = 7.826$ Å, $V = 118.79$ Å^3, respectively.

Microstructure

Figure 5 (a) shows TEM micrographs of the $(LLTaO)_{PS}$ powders fired at different temperatures for 1 h. In the temperature range corresponding to the amorphous region ($T < 900$ K) particles of about 5 nm in size form aggregates, as shown in Figure 5 (a). In the crystallization region ($970\ K < T < 1570$ K) the particle size increases from 15 nm to 140 nm (Figure 5, a). Part b of Figure 5 shows that the size increases linearly with firing temperature. The dilatometric curve shown in Figure 5 (c) reveals that the sintering process occurs at the same time when the grain growth takes place. Sintering begins at 1300 K leading to the shinkage of the pellet and to its compactness. The highest compactness (89%) has been achieved after a sintering at 1570 K for 2 h. Figure 6 shows a TEM image of a ceramic sintered at 1570 K for 2 h and the corresponding electron diffraction pattern. It confirms the good crystallinity of the sample and the absence of an amorphous phase. The powder is made up of grains of 150–200 nm in size with domains due to the cell-parameter values (a_p, a_p, $2a_p$).

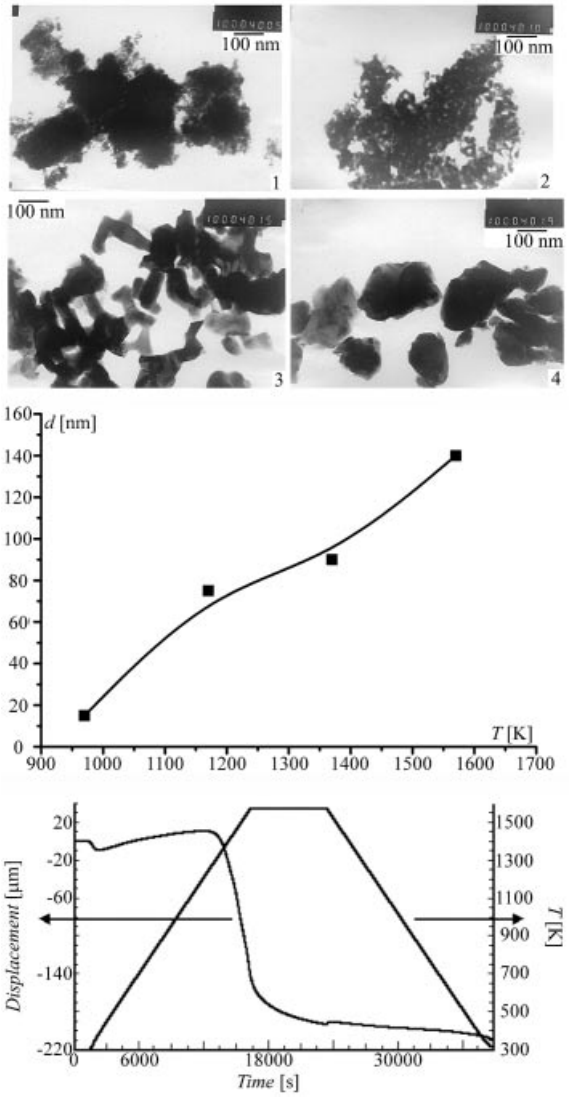

Figure 5. (a) TEM micrographs of the $Li_{0.5}La_{0.5}Ta_2O_6$ powder prepared by the (PS) route [$(LLTaO)_{PS}$)] and fired at different temperatures: (1) 370 K, (2) 970 K, (3) 1170 K, (4) 1570 K for 1 h. (b) Particle average size of the $Li_{0.5}La_{0.5}Ta_2O_6$ powder prepared by the (PS) route [$(LLTaO)_{PS}$] as a function of firing temperatures. (c) Dilatometric curve of a pellet of the $Li_{0.5}La_{0.5}Ta_2O_6$ powder prepared by the (PS) route [$(LLTaO)_{PS}$].

The peculiarities of the precipitation method employed in the synthesis of ceramic materials are known to enable preparation of a mixture of starting reagents at a "molecular level", which facilitates the formation of fine-grained ce-

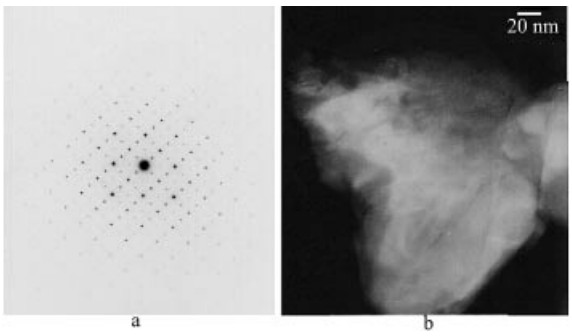

Figure 6. Electron diffraction pattern (a) and the corresponding TEM picture (b) of the $Li_{0.5}La_{0.5}Ta_2O_6$ powder prepared by the (PS) route [$(LLTaO)_{PS}$] fired at 1570 K for 2 h and ground.

ramics. A comparison can be made in Figure 7 that shows the microstructure of $Li_{0.5}La_{0.5}Ta_2O_6$ ceramics obtained by both synthetic methods. Figure 7 (a) shows the microstructure of a ceramic pellet obtained from powders prepared by the (PS) route and sintered at 1570 K for 2 h. It is characterised by a particle size of the order of 200 nm. Figure 7 (b) shows the microstructure of a ceramic pellet obtained by the (SSR) route and sintered at 1770 K for 1 h. A bigger grain size of about 6 μm is observed. Without doubt this result confirms the advantage of the precipitation method to prepare fine-grained ceramics.

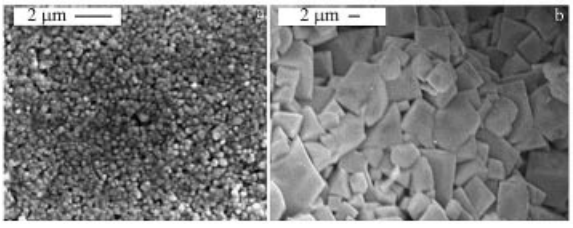

Figure 7. SEM micrographs of a sintered pellet of $Li_{0.5}La_{0.5}Ta_2O_6$ prepared (a) by the (PS) route and fired at 1570 K for 2 h and (b) by the (SSR) route and fired at 1770 K for 1 h.

Electrical Properties of the Sintered Tantalates

For many electrochemical applications the resistance of the grain boundaries as well as the compactness of the sample are important parameters. The resistance of the grain boundaries generally limits the performance of an electrochemical device. To minimise the resistance of the grain boundaries and to increase the compactness of the pellet, sintering has been performed at 1570 K for 2 h for the pellet prepared by the (PS) method and at 1770 K for 1 h for the pellet prepared by the (SSR) route. It is obvious that such different sintering conditions will lead to different grain boundary properties. The electrical properties of these sintered ceramics have been studied by the impedance spectroscopy technique. Figure 8 shows typical impedance spectra obtained at 300 K under dry N_2, for both pellets. In order for comparisons to be made, the real and imaginary parts of the impedance have been normalised according to the geometric factor of the sample (l/s, l = thickness and s = geometric area). The high frequency part of the diagrams ($f > 10$ or 1 kHz) is attributed without doubt to the ionic relaxation in the bulk and the grain boundaries of the oxide. The low frequency part, which appears as a straight line, is attributed to the electrode polarisation. From Figure 8 it can be clearly observed that the total ionic impedance of the PS sample is higher than that for the SSR sample. This overall behaviour is observed for all the temperatures investigated. Figure 9 presents the total ionic conductivity (bulk and grain boundaries) as a function of temperature of sintered samples obtained from either the (SSR) or (PS) route. We attribute the deterioration of the transport properties of the fine-grained sample, prepared by the (PS) method, to an increase of the grain boundary impedance contribution, as previously observed with the 200 nm grain size $Li_{0.30}Ca_{0.35}TaO_3$ synthesised by a polymerised complex route.[20]

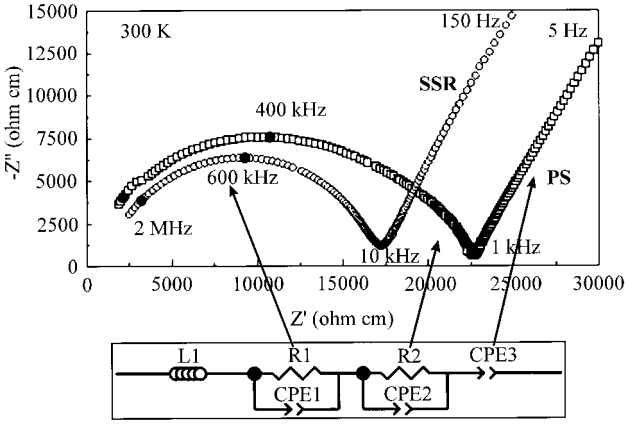

Figure 8. Normalised impedance spectra, recorded at 300 K, of $Li_{0.5}La_{0.5}Ta_2O_6$ prepared by the (PS) route and fired at 1570 K for 2 h and by the (SSR) route and fired at 1770 K for 1 h with the equivalent electrical circuit used for spectra refinement. The normalising factor is the pellet geometric factor (s/l).

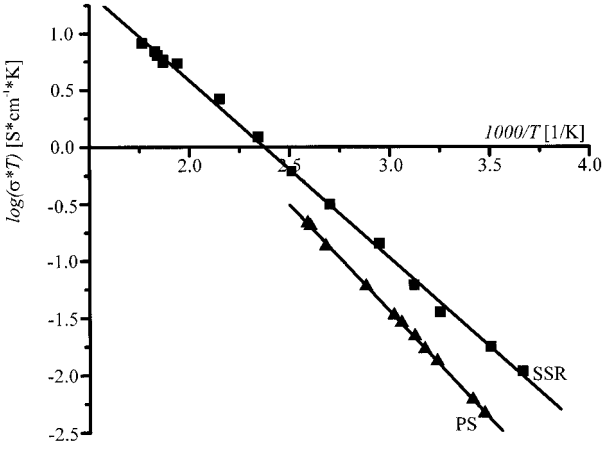

Figure 9. Arrhenius plots of the total ionic conductivity of sintered pellets of $Li_{0.5}La_{0.5}Ta_2O_6$ prepared by the (PS) route and fired at 1570 K for 2 h and by the (SSR) route and fired at 1770 K for 1 h.

In order to evaluate the importance of the grain boundary impedance of the sintered sample obtained by the (PS)

method, we performed the analysis of the impedance diagrams by means of an electrical model. Several possible electrical models were used, which were made up of series and parallel circuits. The model shown in Figure 8, below the impedance diagram, is the one which enabled us to fit all the impedance diagrams in the 175 K to 600 K temperature range. The analysis shows that two relaxations are necessary to fit the "semicircle" of the (PS) sample above room temperature, instead of only one for the (SSR) route. The high frequency relaxation is attributed to the ionic motion of Li^+ inside the grains and the low frequency relaxation to the ionic motion from grain to grain. The bulk conductivity of the sample is easily determined by using the high-frequency resistance R_{Hf}. Figure 10 shows the bulk conductivity, plotted in an Arrhenius fashion for both the (PS) and (SSR) sintered pellets. As found for the titanates,[22] the bulk conductivity is the same for both tantalates confirming that neither the synthesis method nor the grain size influence the nature and consequently the electrical properties of the oxide. On the other hand, the grain boundary resistance varies with the synthetic route. It is negligible when the sample is prepared by the (SSR) route and sintered at 1770 K for 1 h, whereas it becomes important when the sample is prepared by the (PS) route, sintered at 1570 K for 2 h and made up of particles of the order of 200 nm in size. It has to be noted that below room temperature thee relaxations are needed to fit the impedance data of the (PS) sample showing the presence of another electrical barrier that can be attributed to a boundary between the aggregates. The presence of this complex microstructure leads to an increase in the blocking effect and therefore to an increase in the total impedance of the (PS) pellet. This phenomenon has already been observed in $Li_{0.30}Ca_{0.35}TaO_3$[20] and in $Li_{3x}La_{2/3-x}TiO_3$[23] perovskites obtained by the sol-gel route, where both display a microstructure made up of grains and aggregates.

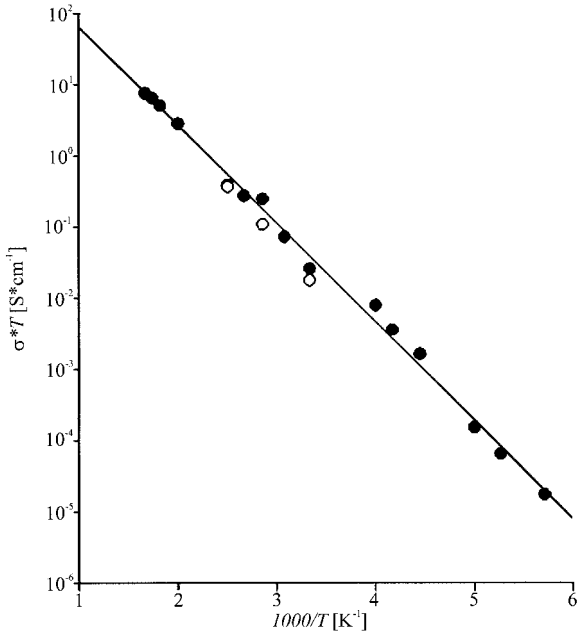

Figure 10. Arrhenius plots of the bulk conductivity of the (PS) ceramic sintered at 1570 K for 2 h (black dots) and of the (SSR) ceramic sintered at 1770 K for 1 h (white dots).

Conclusion

The peculiarities of the preparation of lithium-containing lanthanum tantalates with a defect-perovskite structure using different synthetic methods have been studied. For the solid-state reaction (SSR) method it has been found that the formation of lanthanum metatantalate and lithium-containing lanthanum metatantalates proceeds via the formation of the intermediate phases $LaTaO_4$, $LaTa_5O_{14}$, $LaTa_7O_{19}$ and $LiTaO_3$, $LiTa_3O_8$, $LaTaO_4$, $LaTa_3O_9$, $LaTa_5O_{14}$, respectively. When using the precipitation from solution (PS) route, it has been shown that the precipitate formed is an aquacomplex of the polymeric type. The specific features of the (PS) method enabled the perovskite-phase formation temperature (1020 K) and the sintering temperature (1570 K) to be reduced by 200 K, as compared with the solid-state reaction method (1220 K and 1770 K, respectively). Furthermore, this chemical route facilitates the formation of fine-grained ceramics, even after sintering ($d \approx 200$ nm). The analysis of the impedance data reveals that the Li^+ motion inside the grains is not affected by the synthetic route. However, the complex microstructure of the ceramic obtained by the (PS) route, made up of fine grains and aggregates, leads to an increase of the grain- and aggregate-boundary blocking effect and to a slight decrease of the overall ionic conductivity.

Experimental Section

Extra pure oxides and carbonates, La_2O_3, Ta_2O_5 and Li_2CO_3, were used as original reagents in the synthesis of $(Li_{3x}La_{2/3-x}v_{4/3-2x})$-$Ta_2O_6$ ($3x$ = 0, 0.50, 0.62, 0.74, 1.10, 1.85) by the SSR method. The synthesis and pellet sintering procedures have been described previously in detail.[7,8]

To synthesize $(Li_{3x}La_{2/3-x}v_{4/3-2x})Ta_2O_6$ ($3x$ = 0.5) by the PS method, alcoholic solutions of extra pure $La(NO_3)_3$ and $TaCl_5$ and aqueous solutions of LiOH and NH_4OH were used. The NH_4OH solution was added, at pH 9, to the mixture of $La(NO_3)_3$ and $TaCl_5$ solutions, taken in a stoichiometric ratio. The obtained precipitate was washed with a 2-propanol/distilled water mixture. The LiOH solution was then added to the precipitate, whilst stirring, and the solvents were evaporated. The obtained powder, hereafter named $(LLTaO)_{PS}$, was subjected to thermal treatment over a temperature range 770–1670 K for 1 h.

Differential thermal analysis (DTA), differential thermal gravimetry (DTG) and thermal gravimetry (TG) were performed with a Q-1000 OD-102 device at a heating rate of 10 K·min^{-1}, under dynamic conditions in air, using a Pt crucible. The infrared (IR) spectra were recorded with a Specord-M80 spectrometer over the 200–4000 cm^{-1} frequency range. Samples used for the investigation were prepared as pellets with KBr. Powder X-ray diffraction (XRD) experiments were carried out with a DRON-4-07 diffractometer at room temperature using Cu-K_α radiation (40 kV, 18 mA). The data were recorded using a step-scanning mode in the 2θ range from 10° to

150°, with a step size of 0.02° and an exposure time of 10 s for each point. SiO_2 (2θ standard) and NIST SRM1976-Al_2O_3 (certified intensity standard) were used as external standards.[24] The crystal parameters were refined using the Fullprof Rietveld analysis.

Microstructure studies were performed by scanning electron microscopy (SEM) using a JEM 10CX II (JEOL) electron microcope. Transmission Electron Microscopy (TEM) was also performed. Thin specimens for the TEM study were obtained by ultrasonically dispersing particles in ethanol and depositing one drop of the resulting suspension onto a Cu grid covered with a holey carbon film. After drying, the grid was fixed in a side-entry ±30° double-tilt specimen holder and introduced into a JEOL-2010 electron microscope operating at 200 kV.

A dilatometric experiment was performed with a vertical dilatometer (Setsys Evolution 1750 TMA equipment from Setaram). The dilatometer follows the continuous axial shinkage of the studied pellet as a function of temperature. Experiments were carried out in air with a 5 K·min^{-1} sweep rate, from ambient temperature to 1570 K. This constant temperature was maintained for 2 h and then cooling to room temperature was performed at the same sweep rate as above. The probe used was that of an aluminium hemisphere. The density of the sintered pellets was estimated from the mass and the geometric dimensions of the sample. The compactness after sintering was then evaluated from the density, the molar mass and the cell parameters of the compound.

The electrophysical properties of the ceramic samples after sintering were investigated by complex impedance spectroscopy in the frequency range 1–10 MHz using a 1260 Frequency Response Analyzer and a 1296 Dielectric Interface from Solartron. The measurements were performed over the temperature range 135–600 K under vacuum at low temperature in a cryogenerator and under dry N_2 above room temperature in an oven (Dataline). We checked that the electrochemical system remains linear up to 1 V (rms), and therefore the applied ac voltage was 400 mV (rms).

The pellets were obtained from powders resulting from either the solid-state reaction or precipitation from the solution. The powders obtained from the (SSR) technique were pressed into pellets and then sintered for 1 h at 1700–1770 K in air. The powder obtained from the (PS) route [$(LLTaO)_{PS}$] was first mixed with an organic binder (Rhodoviol®) to prevent the breaking of the pellet owing to the presence of very fine grains. Pellets were then prepared by first pressing the powder uniaxially at ≈250 MPa and later pressing it isostatically at ≈500 MPa. The pellet was then heated at 670 K for 12 h in air to decompose the organic binder and then sintered for 2 h at 1570 K (with a sweeping rate of 5 K min^{-1}). Sputtered Pt films were deposited onto the pellets and used as ion-blocking electrodes in the measurement of the ionic conductivity. The same electrical model as described in ref.[22] was used to determine the bulk conductivity and the grain boundary conductance.

Acknowledgments

We thank M.-P. Crosnier-Lopez for the help with the TEM micrograph and electron diffraction pattern of Figure 6.

[1] A. Belous, G. Novitskaya, S. Polianetskaya, Y. Gornikov, *Izv. Akad. Nauk SSSR. Neorg Mater.* **1987**, *23*, 470–472.
[2] Y. ınaguma, C. Liquan, M. Itoh, T. Nakamura, T. Uchida, H. Ikuta, M. Wakihara, *Solid State Commun.* **1993**, *86*, 689–695.
[3] O. Bohnké, J. Emery, J. L. Fouquet, J. Badot, *Recent Research Developments in Solid State Ionics* (Ed.: S. G. Pandalai), Transworld Research Network Publishers, ISBN 81–7895-069-3, **2003**, *1*, 47.
[4] A. Belous, I. Didukh, E. Novosadova, Y. Pashkova, *Phys. Solid State* **1986**, *28*, 3230–3232 (in Russian).
[5] K. Mirumoto, S. Hayashi, *J. Ceram. Soc. Jpn.* **1998**, *106*, 369–371.
[6] K. Mirumoto, S. Hayashi, *Solid State Ionics* **1999**, *116*, 263–269.
[7] O. Gavrilenko, A. Belous, Y. Pashkova, V. Mirnyi, *Neorg. Mater.* **2002**, *38*, 1126–1130.
[8] A. Belous, Y. Pashkova, O. Gavrilenko, O. V'yunov, L. Kovalenko, *Intern. Journal of Ionics* **2003**, *9*, 21–27.
[9] I. Vasserman, *Chem. (Leningrad)* **1980**, 207 (in Russian).
[10] L. Komissarova, V. Shatskii, G. Pushkina, *Nauka (Moscow)* **1984**, 234 (in Russian).
[11] K. Nakamoto, *Mir (Moscow)* **1991**, 320 (in Russian).
[12] Powder Diffraction File **1997**: PDF-2, *Database Sets*, 47.
[13] K. Portnoi, N. Timofeeva, S. Salibekov, *Neorg. Mater.* **1970**, *6*, 289–293.
[14] P. Arsenyev, V. Glushkova, A. Yevdokimov, *Nauka (Moscow)* **1985**, 261 (in Russian).
[15] Y. Isupova, R. Pomes, Y. Savchenko, E. Keler, *Neorg. Mater.* **1975**, *11*, 384–386.
[16] Q. Pham, C. Bohnké, J. Emery, O. Bohnké, F. Le Berre, M. Crosnier-Lopez, J. Fourquet, P. Florian, *Solid State Ionics* **2005**, *176*, 495.
[17] J. Fourquet, H. Duroy, M. Crosnier-Lopez, *J. Solid State Chem.* **1996**, *127*, 283–294.
[18] A. Sych, T. Novik, L. Yeryomenko, V. Kushkov, *Ukr. Khim. Zhurn.* **1978**, *44*, 794–798.
[19] T. Panova, E. Keler, *Zhurn. Neorg. Khim.* **1975**, *XXI*, 815–820.
[20] Q. Pham, M. Vijayakumar, C. Bohnké, O. Bohnké, *J. Solid State Chem.* **2005**, *178*, 1915–1924.
[21] A. Belous, E. Pashkova, O. Gavrilenko, O. V'yunov, L. Kovalenko, *Ionics* **2003**, *9*, 21–27.
[22] A. Belous, O. Yanchevskiy, O. V′yunov, O. Bohnke, C. Bohnke, F. Le Berre, J. Fourquet, *Chem. Mater.* **2004**, *16*, 407–417.
[23] M. Vijayakumar, O. Bohnké, *J. Eur. Ceram. Soc.*, in press.
[24] Certificate of Analysis, Standard Reference Material **1976**, Instrument Sensitivity Standard for X-ray Powder Diffraction, National Institute of Standards & Technology, Gaithersburg, **1991**, 4.

Received: July 26, 2005
Published Online: March 1, 2006

